Methods to analyze imaging radio data on solar flares

Victor V. Grechnev *
Institute of Solar-Terrestrial Physics, Lermontov Street 126, Irkutsk 664033, Russia
grechnev@iszf.irk.ru

Abstract

Putting additional constraints on physical conditions based on the observed quantities, microwave imaging data crucially enhance reliability of results and consistency of interpretations. This is why microwave imaging data is a necessary constituent of observational data sets on solar flares, and they are widely used in their analyses. At the same time, to identify essential features and study their behavior, one has to deal with large data sets of hundreds frames. However, this allows a single image, a variance map, that represents overall dynamics of the event. In this review, methods are presented that allow identification of active flare sources in large data cubes and investigation of the detected positions of sources in both Stokes I and V images using analyses of variance maps, combined difference images, and total flux time profiles. By analyzing the similarity of time profiles for different-polarity Stokes V sources, one can reveal magnetic connectivity. Imaging techniques at the NoRH in both the local and remote modes as well as interactive data analysis using IDL are also briefly discussed.

Key words: Sun: radio radiation — Sun: flares — methods: data analysis — techniques: image processing

1. Introduction

Comprehensive data sets in various emissions on an event under investigation put several observational constraints on physical conditions and scenarios considered. Analyzing them, one loses freedom to speculate, but gains confidence in that the estimates obtained from various observations using different methods are reliable, the interpretation is robust, and this everything is consistent with many observational facts. When studying solar flares, one has to analyze both thermal and non-thermal emissions. Whereas thermal emissions (e.g., soft X-rays, extreme ultraviolet) show fine spatial structures of flare regions and their vicinity, non-thermal emissions (primarily hard X-rays) provide information on high-energy particles accelerated in flares. Being responsive to both thermal and non-thermal flare manifestations, microwave imaging data are widely used in analyses of solar flares. Being highly sensitive to magnetic fields, radio observations give a unique method of identifying magnetic configurations and estimating magnetic field strengths in the corona. Well known are facts when it is not possible to disclose all important flare sources without microwave observations (e.g., in cases of strongly asymmetric loops—Kundu et al. 1995). In addition, microwave images have wide dynamic range (> 100 for NoRH and can be still improved using optimal weighting of visibilities, while it was ~ 10 for *Yohkoh*/HXT). All these convince that microwave observations of solar flares are quite necessary, rather than supplementary only.

Typical tasks to be solved in analyses of solar flares are: a) to identify active flare sources, b) to find out their nature and emission mechanisms, and c) to relate their properties with parameters of plasmas and accelerated particles in flaring regions, i.e., to constrain physical conditions based on the observed quantities.

Most microwave imaging data on solar flares have been come during the last decade from the Nobeyama Radioheliograph (NoRH, Nakajima et al. 1994). Besides images, NoRH produces correlation plots, which sample small spatial scales by using combined responses from the longest baselines of the radio interferometer. A researcher who is going to use NoRH imaging data must first produce a set of images ("data cube") from raw data, and then to identify active flare sources.

Known ways to reveal flaring sources involve 1) analyses of "base" (Kundu et al. 1995) or "running" difference images (Delannée et al. 2000), 2) viewing in the movie mode, and 3) analyses of time profiles along several check points of a data cube (Hanaoka et al. 1994). However, all of them are insufficiently efficient and have some other weak points. Therefore, studies of solar flares involve time-consuming, laborious processing and analyzing large sets of images. Here, methods are described, which involve a set of techniques that allow efficient identifying short-term features in imaging data (Grechnev 2003). *The methods were developed primarily for analyses of NoRH data.*

2. Essence

2.1. Choice of the time interval for imaging

NoRH correlation plots can be used for that. Correlation plots can be misleading if the spatial structure is complex, but they show temporal variations of compact features. Then the image set over the whole time interval

* The essence of the methods was developed in NRO, when V. Grechnev was a Foreign Research Fellow of NAOJ

chosen is produced with a required cadence.

2.2. Search for active flaring sources

Robertson (1991) first proposed to use variance imaging in radio astronomy. Then r.m.s. images were used by Tsiropoula, Alissandrakis & Mein (2000), and Nindos et al. (2002) in studies of quasi-periodic oscillations. Variance maps (or r.m.s. images) can be also successfully used to find important flare sources. The variance maps are computed by calculating variance of every spatial point of the data cube along its temporal dimension. The variance map presents the dynamics of the entire event, with the value of each its point showing the temporal variability of the corresponding spatial point. Therefore, variable sources that change their brightness, position, etc. come into view in the variance map—of course, according to the statistical importance of their variability. For reasons of computational efficiency, I calculate the variance (r.m.s.) map σ_{ij}^2 for a data cube x_{ijk} using the expression

$$\sigma_{ij}^2 = 1/N \sum_{k=1}^{N} x_{ijk}^2 - 1/N^2 \left(\sum_{k=1}^{N} x_{ijk} \right)^2$$

where $k = 1, 2, \ldots, N$ is the number of the image "layer" in the data cube. This expression is equivalent to the definition of the variance (see, e.g., Cramér 1946), but does not contain cross terms, which decreases the computational time.

Images to be analyzed using variance maps must be well calibrated and coaligned. The variance map catches such problems of an image set. The effect of random shifts less than the size of a source is a ring-shaped response in the variance map, with "darker" middle and "brighter" strip along the edge. The effect of jumps between few fixed positions well exceeding the size of the source is appearance of false additional sources.

If the considered interval is so long, that the solar rotation becomes important, it should be compensated, or other precautions should be undertaken. Otherwise, there is enough time for significant displacements of quiet sources, and this inevitably results in their artifactitious appearance as strongly variable duplicated sources.

2.3. Time profiles of flaring sources

When active flare sources are identified and selected, I analyze their time profiles separately by integrating pixel values over small areas covering the sources entirely. The total flux time profiles are computed for each source as $S_{[sfu]} = 2k\,(\nu/c)^2 \sum_i T_{Bi}\,\Delta\Omega = 7.22 \times 10^{-11}\ \nu_{[GHz]}^2\ \rho_{[arcsec]}^2 \sum_i T_{Bi[K]}$, with k being Boltzmann constant, c speed of light, $T_{Bi} = (R_i + L_i)/2$ brightness temperature of each pixel (with a linear size of ρ), ν frequency, and $\Delta\Omega$ solid angle corresponding to one pixel of the image.

Next, when prominent features in the time profiles are found, I produce detailed image sets with as short time interval between them as necessary. Then variance maps are used again, and this process can be repeated iteratively, until the whole dynamics of the spatial structure is revealed. The iterations are performed to reveal all important sources and to compute the time profiles for each of them as detailed as the physical task requires.

2.4. Magnetic connectivity

To identify magnetic connectivity, one can use the fact that the gyrosynchrotron emission from a flare loop at 17 GHz usually is conspicuously polarized, and the sign of the polarization must be opposite in conjugate footpoints of a flare loop (if there is no polarization reversal, which can be expected at 17 GHz to be close to the limb). In addition, when one deals with a particular flare loop, then the same electron population is likely responsible for the emissions from both footpoints; hence, their time profiles may be expected to be similar in shape (but not in either flux or brightness temperature values). Hence, one can try to identify magnetic connectivity of the detected regions by comparing various time profiles computed for the Stokes V component in all the regions, and finding those, that match in local peaks and have the opposite polarization (note, however, that it is not always possible). Difference images are also useful here, as produced in the following way. First, some images taken during a peak are averaged. Then another image is composed from frames taken before the peak and/or after it. Finally, the latter image is subtracted from the former one. (This way can be applied to both Stokes V and I images.) The next step is the comparison of time profiles for loop footpoints found.

When events with simple spatial structure are analyzed, this approach is quite straightforward. Moreover, sometimes magnetic connectivity can be revealed even from the analysis of the total intensity time profiles as Hanaoka (1999), Kundu et al. (2001), and Grechnev & Nakajima (2002) did. In more complex cases, the way described can become rather sophisticated; nevertheless, using just this way, Grechnev, Kundu & Nindos (2004) succeeded to follow formation of a post-eruptive arcade in a long-duration eruptive event of February 16, 1999.

2.5. Spectral index

When dealing with radio maps produced by NoRH, one can study data at two operating frequencies of 17 and 34 GHz. Taking into account that these frequencies usually belong to the optically thin high-frequency part of the microwave burst spectrum, note that the flux density of the thermal bremsstrahlung is almost the same at these two frequencies, whereas gyrosynchrotron emission from high-energy electrons has a rather steep spectral slope. These two emission mechanisms are dominant for flaring sources at these frequencies (gyrosynchrotron emission in the impulsive phase and free-free emission in the decay phase). It is easier to identify the emission mechanism for a microwave source if one knows the spectral index of its emission α, which can be calculated from two-frequency data.

One can compute the spectral index as $\alpha = \log(S_L/S_H)/\log(\nu_H/\nu_L)$ with S_ν being flux density measured at the frequency of ν, and subscripts "*F*" and "*H*" denote the higher and lower frequencies. To estimate the spectral index correctly, the difference in the beam sizes at the two frequencies should be compensated. One can do this, following Nobeyama Solar Group, by convolving 17 GHz images with the NoRH beam pattern at 34 GHz, and by convolving 34 GHz images with the NoRH beam pattern at 17 GHz.

2.6. Thermal contribution

Thermal bremsstrahlung in microwaves can be found from soft X-ray data (e.g., *Yohkoh*/SXT, *GOES*): $S_{[sfu]} \approx 3 \times 10^{-45} EM_{[cm^{-3}]} T_{[K]}^{-1/2}$, where EM and T are emission measure and temperature of the observed source. In a similar way, a simulated microwave "image" in optically thin free-free emission can be computed using column EM and T_e distributions inferred from soft X-ray imaging data (e.g., from *Yohkoh*/SXT images—see, e.g., Grechnev et al. 2004b).

3. Examples

This sections demonstrates the capability of the variance method by considering examples of 17 GHz data analyses for two impulsive flare events recorded with NoRH.

3.1. Event of December 22, 1999

An impulsive solar flare of December 22, 1999 occurred in the active region 8807 (N17 E15) during 01:50–02:37 UT with a peak of M1.8 at 02:16 UT according to *GOES*. The spatial and temporal structure of the flare microwave emission was complex. However, the rise phase of the event had rather simple structure, and it is convenient to use it as an example to show what we gain from variance maps.

The image set to be analyzed consists of *167* 17 GHz snapshots produced using *Fujiki program*[1] with an interval of 1 sec. This imaging software provides higher spatial resolution. Figure 1a shows an averaged image of the flare region of $314'' \times 314''$ composed from the whole image set. Several microwave sources can be seen in this image: compact sources 1, 2, and 3 as well as a faint extended feature 4 in the northern (upper) part of the frame. Note that the source 3 is the brightest one here.

The variance map computed from the same set of *167* images is shown in Fig. 1b. One can see here, however, that the most prominent is source 1; source 2 is weaker; and no more bright sources are detectable. To investigate behavior of the sources, we extract three regions in the images using the masks shown in Fig. 1a as dashed contours. The time profiles of the variable parts of the total flux emitted by sources 1, 2, and 3 are shown in Fig. 2 along with the whole total flux computed from the entire frames.

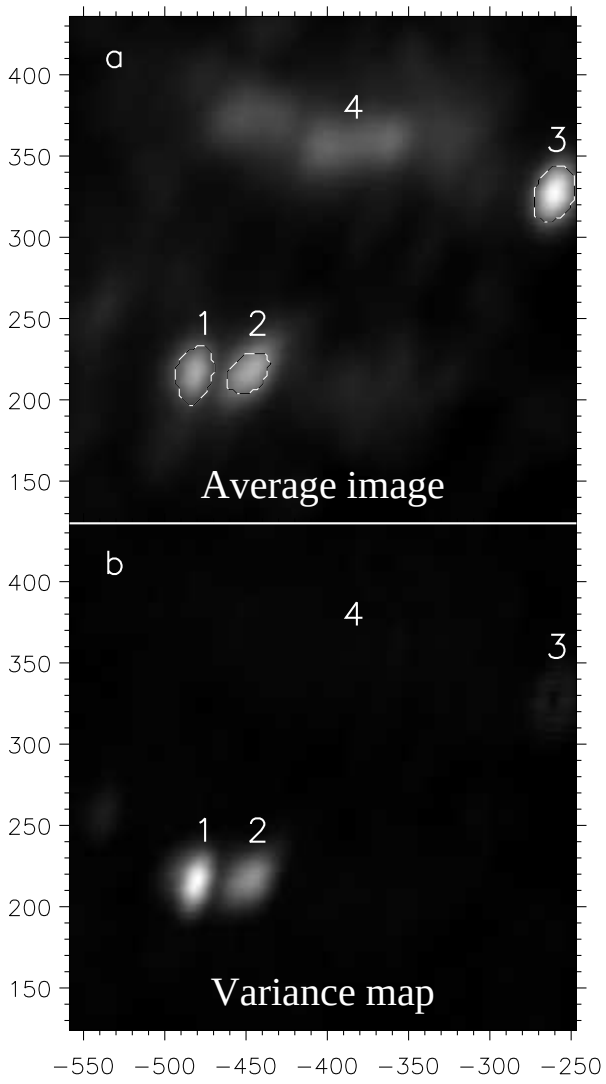

Fig. 1. The initial stage of December 22, 1999 event: **a** the image produced by averaging of all *167* 17 GHz NoRH frames within the analyzed interval; **b** the variance map computed from this set. The masks to select the most prominent sources 1–3 are shown in panel **a** as dashed contours, and time profiles of the sources are shown in Fig. 2. Axes show arc seconds from the solar disk center. Both images are shown non-linearly, at the power of 0.8.

[1] see http://solar.nro.nao.ac.jp/norh/doc/manuale/index.html

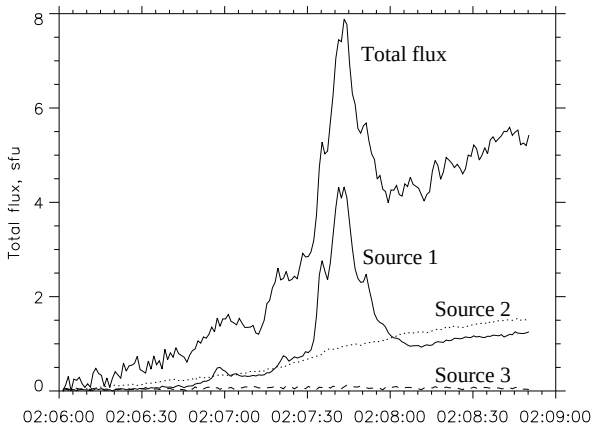

Fig. 2. Total flux time profiles for three sources shown in Fig. 1 along with the whole total flux computed from the entire frames. Minimum values of all time profiles are subtracted.

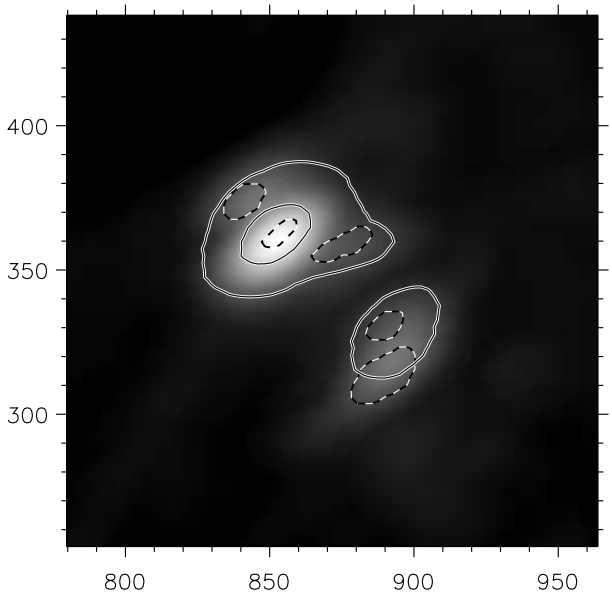

Fig. 3. The variance map computed from *231* NoRH 17 GHz images for November 10, 1998 event. The interval of the computation is from the thick "dash–three dots" line shown in Fig. 8 up to the end of the record. Five active sources (dashed contours) can be revealed from the variance map, while the image at the peak of the second burst (the instant labeled large "C" in Fig. 5) shows two sources only (solid contours at [0.05, 0.5] of the maximum). Axes show arc seconds from the solar disk center.

The situation visible in the variance map essentially differs from the picture shown by the average image. The strongest source 3 is not visible because it is almost unchanged: its brightness temperature is 0.22 MK, and the variations do not exceed 30 000 K. Source 1 is of the highest variability, although in the average image it is weaker than both sources 2 and 3, and we can really see in Fig. 2 that its behavior is the most impulsive. Its brightness temperature reaches 0.7 MK, whereas the brightness temperature of source 2 is $T_B \leq 0.25$ MK. The extended northern brightening (4) with $T_B = 80\,000 \pm 15\,000$ K does not show any detectable variability; hence, it is not detectable in the variance map.

This example shows that the major impulsive processes in early beginning of the flare were associated with source 1, which was likely non-thermal. The similarity of the smoother background of source 1 with the time profile of source 2 suggests their probable connection. However, the strongest, likely gyroresonance, source 3 had no relation to active processes during the event.

3.2. Event of November 10, 1998

More complex spatial and temporal structures are exemplified by the well-known flare event of November 10, 1998, first presented by Asai et al. (2001). The event actually included a train of four bursts, in the second of which pulsations with an extraordinarily high modulation depth were observed. For the first glance, two flare sources were present in 17 GHz images of the event, in particular, in its pulsating part. However, the spatial structure contained more features in the reality.

Figure 3 shows a variance map computed from a 1-sec set of *231* NoRH snapshots observed during the interval to cover three last bursts (from thick "dash–three dots" line in Fig. 5 up to the end of the record). Two prominent microwave sources observed at one of peaks of the pulsating burst are shown on top of the halftone background by solid contours, but careful examination allows detecting five variable regions marked with dashed contours in the figure. Note that the sizes of these regions were selected from reasons of their separation rather than to cover the sources entirely. This is why in Fig. 5 just the average brightness temperatures are shown rather than the total fluxes.

Figure 4 shows 17 GHz images of the event for four times. Dashed contours show **five** active flare sources 1–5 revealed by the variance method. The time profiles of those sources are shown in Fig. 5. In the light curves, we can select some representative moments when some features show up. By subtracting from images corresponding to those moments (solid lines and capital letters) other images, before those features (broken lines and the corresponding small letters), we obtain a picture of microwave sources responsible for those features in the time profiles.

Next, we come back to Fig. 4. Halftone background in *left column* shows *non-subtracted* images, while *right column* shows *subtracted* images. So, we see in right column those sources, which were responsible for the brightenings **B**, **C**, and **D** as well as the long decay **A**.

This event was studied in more detail by Grechnev, White & Kundu (2003).

4. Technical details

I perform all data handling in IDL[2] environment, which is the most common for the solar community. All routines

[2] IDL is the trademark of Research Systems, Inc. http://www.rsinc.com

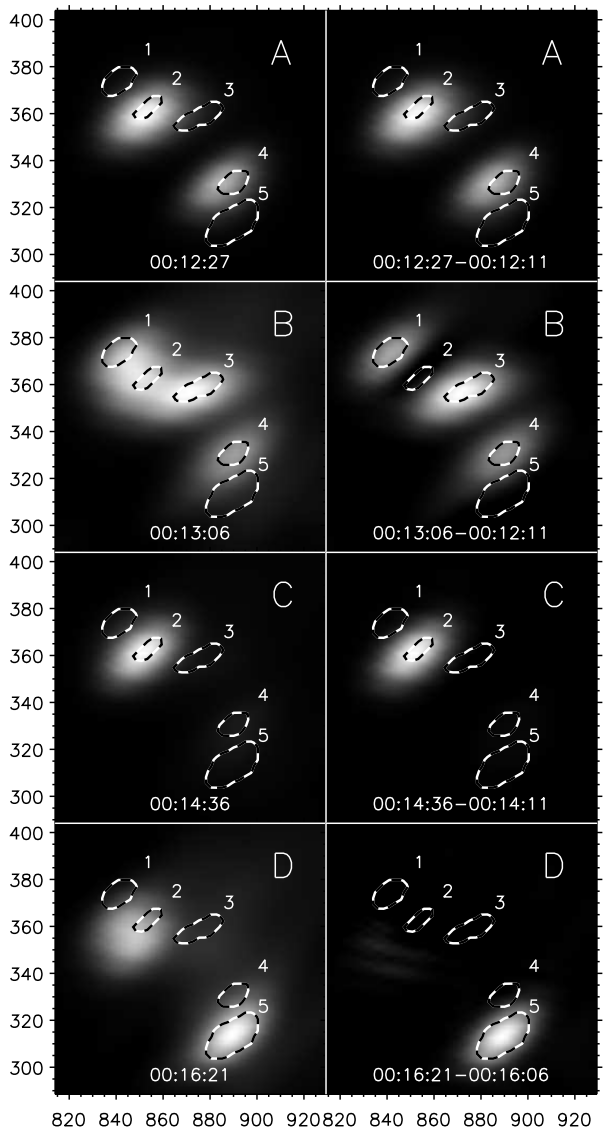

Fig. 4. NoRH 17 GHz images of November 10, 1998 event. Left column shows 17 GHz images observed at some characteristic times labeled with capitals "A"–"D" in Fig. 5. Right column shows *difference* images produced by subtraction from images in the left columns another ones, observed at times labeled with the corresponding small letters "a"–"d" in Fig. 5. Active sources revealed by the variance map are shown by dashed contours. Axes show arc seconds from the solar disk center.

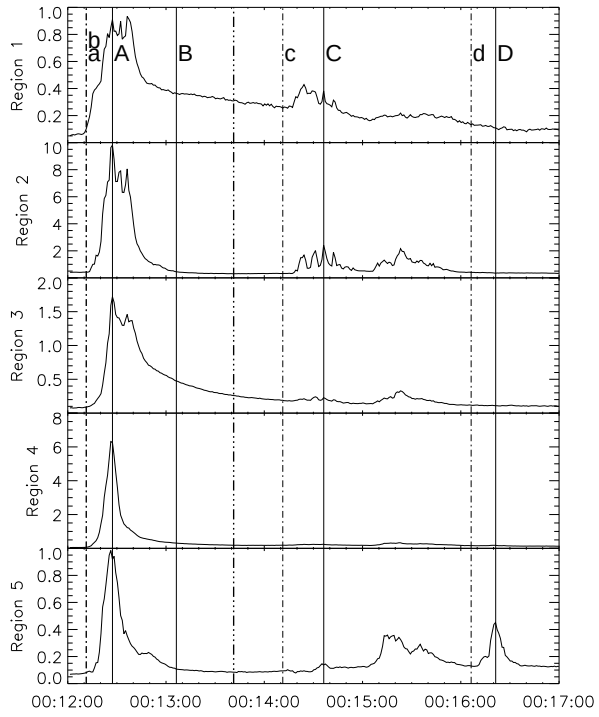

Fig. 5. NoRH 17 GHz time profiles of average brightness temperatures (MK) over the regions labeled 1–7 in Fig. 4

hereinafter refer to IDL.

4.1. Imaging

To produce images from raw NoRH data, I use the routine **norh_synth** developed by T. Yokoyama that provides an interface to fill in parameter files for an imaging software, and starts the running of the program. In my code, I arrange some environment in addition to this routine, and create the parameter file with a unique name formed from the system time. This allows several imaging jobs to be queued simultaneously. This way can be used in both the local mode, in Nobeyama, and the remote mode—elsewhere in the world (using access via secure shell, **ssh**).

4.2. Manipulation with Graphics without Graphical Output

To perform routines that need graphical output (e.g., **MAP_SET** when working with the orthographic projection) *in the remote mode without access to X Windows display*, one can use the **Z** buffer graphics device. I give below a simple example to show how to find heliographic coordinate of the brightest point in a NoRH image using built-in IDL routines.

```
data = readfits(filename, header)
Sz = size(data)
init_device = !d.name
set_plot, 'Z'
device, set_resolution = Sz[[1,2]]
X0=sxpar(header,'crval1')/sxpar(header,'cdelt1')
```

```
Y0=sxpar(header,'crval2')/sxpar(header,'cdelt2')
Centvr=[sxpar(header,'crpix1')–X0, $
    sxpar(header,'crpix2')–Y0]
Radius=sxpar(header,'solr')/sxpar(header,'cdelt1')
map_set, sxpar(header, 'solb'), 0, 0, /ortho, $
    position = [0,0,1,1]
!x.s=[Center[0], Radius] / float(!d.x_size)
!y.s=[Center[1], Radius] / float(!d.y_size)
amax = max(data, imax)
print, convert_coord(imax mod Sz[1], $
    imax/Sz[1], /dev, /to_data)
set_plot, init_device
```

The way to control the **MAP_SET** routine used here was proposed by Stern (1997).

4.3. Analysis and Visualization

To analyze three-dimensional data cubes, I developed IDL routines and functions **varmap**, **timeprof**, **total_flux** and some others, which can be found at the Web site http://ssrt.iszf.irk.ru/idl.

A variance map for the array **x** can be computed using a simple IDL code:

total(x∧2, 3)/N – total(x, 3)∧2/N∧2),

which is performed by my function **varmap**. By calculation of the mean value over a quiet (dark) non-zero region in the variance map, one can find the instrumental sensitivity appropriate for the data cube under consideration. Everything below this level can be simply zeroed.

The variability of major non-thermal flare sources is strong; hence, to detect all features of interest, it is useful to display variance maps non-linearly. At the first step, the histogram-equalized transformation can be used to reveal as much variable regions as possible:

tvscl, hist_equal(image)

This drastically decreases the contrast, and both bright and faint features become visible. Next, I apply a power-law display (for example, with a power of 0.3):

tvscl, (image > 0)∧0.3

or, for bipolar images,

tvscl, (image > 0)∧0.3 – (–image > 0)∧0.3

This operation is performed by my function **magpower**, which is convenient, if the **image** itself is some expression also.

Regular instrumental contributions (e.g. sidelobes of the beam pattern) also show up in the variance map. This allows judging whether a source can be due to an instrumental effect, if it is located in the sidelobe region and resembles variations of the major source responsible for these sidelobes.

4.4. Selection of Sources

Prominent sources can be selected using various ways. If a source is strong and isolated, it can be easily detected in a particular frame, or in an averaged image. If it is not so strong, then a variance map can be used to detect it. To form the mask for a particular source, discrimination above some threshold can help, for example,

s1 gt max(s1)*0.4

produces the mask to embrace the source **s1** by the level of 0.4. To separate merged sources, the morphological erosion operator can be used (the **erode** IDL function). Separation of several sources can be performed using the **label_region** built-in IDL function.

After that, time profiles over the regions found can be computed using the **total_flux** function.

Some remarks about interactive data analyses using IDL can be found at the Web site: http://srg.bao.ac.cn /weihailect/Grechnev/Grechnev01.htm.

5. Concluding Remarks

Studies of microwave data on solar flares involve laborious processing and analyzing large three-dimensional data arrays, which can be expedited using the methods outlined.

I developed the essence of the methods and started to use them when studied the impulsive solar flare of September 17, 1999 (Nakajima & Grechnev 1999; Grechnev & Nakajima 2002). Taking advantages of those methods, we were able to analyze large image cubes and to reveal faint impulsive sources, which turned out to be important in understanding flare processes. Further, using those methods, cursory analyses of some dozens of solar flares have been carried out. Some of studies that were more comprehensive have been already published (Kundu & Grechnev 2001, Kundu et al. 2001; Garaimov & Kundu 2002).

The methods can be also used in investigating variable objects in other images. In particular, the variance method was successfully used by Kundu et al. (2001) to study evolution of photospheric magnetic fields. The methods can be also helpful when multi-frequency radioheliographs, which are currently under development (e.g. FASR), start observing the Sun, and data anticipated will well exceed those we deal with so far.

Acknowledgments. The author thanks A. Uralov, A. Altyntsev, H. Nakajima, M. Kundu, and V. Garaimov for fruitful discussions, examination, and the first usage of the method. This work was partly supported by INTAS under grant No. 00-00543 as well as by the Russian Foundation of Basic Research under grants 03-02-16591, 03-02-16229, 03-07-90054, 02-02-39030-GFEN, and the Ministry of Education and Science under grant NSh-477.2003.2.

References

Asai A., Shimojo M., Isobe H., Morimoto T., Yokoyama T., Shibasaki K., Nakajima H. 2001, ApJL 562, L103.

Crámer H. 1946, Mathematical methods of statistics. Princeton, Princeton University Press.

Delannée C., Delaboudinière J.-P., Lamy P. 2000, A&A 355, 725

Garaimov V.I., Kundu M.R. 2002, Sol. Phys. 207, 355

Grechnev V.V. 2003, Sol. Phys. 213, 103

Grechnev V.V., Nakajima H. 2002, ApJ 566, 539

Grechnev V.V., White S.M., Kundu M.R. 2003, ApJ 588, 1163
Grechnev V.V., Kundu M.R., Nindos A. 2004, A Study of Accelerated Electrons in Solar Flares from Nobeyama, Yohkoh, and Other Observations. Nobeyama Symp. 2004 "Solar Physics with the Nobeyama Radioheliograph", http://solar.nro.nao.ac.jp/meeting/nbym04/index.html; PASJ, 2005, in preparation
Grechnev V.V., Borovik V.N., Bugaenko O.I., Bogachev S.A., Grigorieva I.Y., Kuzin S.V., Lesovoi S.V., Livshits M.A., Pertsov A.A., Rudenko G.V., Slemzin V.A., Stepanov A.I., Shibasaki K., Uralov A.M., Zandanov V.G., Zhitnik I.A. Observations of a posteruptive arcade on October 22, 2001 with CORONAS-F, other spaceborne telescopes, and in microwaves. Nobeyama Symp. 2004 "Solar Physics with the Nobeyama Radioheliograph", http://solar.nro.nao.ac.jp/meeting/nbym04/index.html; 2005, PASJ, in preparation
Hanaoka Y., Kurokawa H., Enome S. et al. 1994, PASJ 46, 205
Hanaoka Y. 1999, PASJ 51, 483
Kundu M.R., Nitta N., White S.M. et al. 1995, ApJ 454, 522
Kundu M., Grechnev V. 2001, Earth, Planets and Space 53(6), 585
Kundu M.R., Grechnev V.V., Garaimov V.I., White S.M. 2001, ApJ 563, 389
Nakajima H., Nishio M., Enome S., Shibasaki K., Takano T., Hanaoka Y., Torii C., Sekiguchi H., Bushimata T., Kawashima S., Shinohara N., Irimajiri Y., Koshiishi H., Kosugi T., Shiomi Y., Sawa M., Kai K. 1994, Proc. IEEE 82(5), 705
Nakajima H., Grechnev V.V. 1999, Proc. Yohkoh 8th Anniversary Symp., Explosive Phenomena in Solar and Space Plasma. Ed. Kosugi, T., Watanabe, T., Shimojo, M. (Sagamihara: ISAS), p119
Nindos A., Alissandrakis C.E., Gelfreikh G.B., Bogod V.M., Gontikakis C. 2002, A&A 386, 658
Robertson J.G. 1991, Australian J. Phys. 44, 729
Stern D. 1997, Private communication
Tsiropoula G., Alissandrakis C.E., Mein P. 2000, A&A 335, 375